DEPARTMENT OF DEFENCE
DEFENCE SCIENCE & TECHNOLOGY ORGANISATION

DSTO

Thermographic Assessment of the Heat Dissipation Associated with Fatigue Crack Growth in Mild Steel

N. Rajic

DSTO-TR-1190

20011026 122

Thermographic Assessment of the Heat Dissipation Associated with Fatigue Crack Growth in Mild Steel

N. Rajic

Airframes And Engines Division
Aeronautical and Maritime Research Laboratory

DSTO–TR–1190

ABSTRACT

This report examines the feasibility of predicting rates of crack growth in mild steel based on an evaluation of the crack tip dissipated energy. A numerical scheme is developed to provide a basis for the computation of dissipated power from measurements of temperature acquired using remote infrared detection. An experimental study is then described where measurements of crack-growth rate in mild-steel coupons exposed to constant amplitude cyclic loading are related to calculations of power dissipation. A simple linear relationship is indicated, with testing also providing some evidence of geometry independence, a key finding with regard to the possible use of dissipated energy as a fatigue characterisation parameter. However, further testing involving a more complex loading sequence led to a noticeable change in relationship indicating that the heat dissipation rate is unlikely to offer a simple basis for the prediction of crack growth rate under all loading conditions.

APPROVED FOR PUBLIC RELEASE

DEPARTMENT OF DEFENCE
DEFENCE SCIENCE & TECHNOLOGY ORGANISATION **DSTO**

AQ FO2-01-0082

APPROVED FOR PUBLIC RELEASE

Thermographic Assessment of the Heat Dissipation Associated with Fatigue Crack Growth in Mild Steel

EXECUTIVE SUMMARY

The continued assurance of aircraft structural integrity relies in part on the accuracy of predictions of the rate of growth of cracks in structurally-critical members of an airframe. When based on the stress intensity factor such predictions occasionally fail, often as a result of the inability of the analysis to account for plastic behaviour at the crack tip. In response to this shortfall, alternative analysis techniques have been developed which better account for the role of crack tip plasticity in the crack propagation process.

This report examines the feasibility of predicting rates of crack growth in mild steel based on an evaluation of the crack tip dissipated energy. A numerical scheme is developed to provide a basis for the computation of dissipated power from measurements of temperature acquired using remote infrared detection. An experimental study is then described where measurements of crack-growth rate in mild-steel coupons exposed to constant amplitude cyclic loading are related to calculations of power dissipation. A simple linear relationship is indicated, with testing also providing some evidence of geometry independence, a key finding with regard to the possible use of dissipated energy as a fatigue characterisation parameter. However, further testing involving a more complex loading sequence led to a noticeable change in relationship indicating that the heat dissipation rate is unlikely to offer a simple basis for the prediction of crack growth rate under all loading conditions.

Author

Nik Rajic
Airframes and Engines Division

Nik Rajic recieved a B. Eng. (Hons.) in Mechanical Engineering from the University of Melbourne in 1989. He joined Structures Division at the Aeronautical Research Laboratory in 1991 and in 1992 undertook studies at Monash University which led to the completion of a PhD in 1995. He has since contributed to research on fatigue-life extension techniques, thermoelastic stress analysis, thermoplasticity, thermographic nondestructive evaluation, and insitu structural health monitoring techniques based on smart structures principles. He is currently a Senior Research Scientist in the Airframes and Engines Division.

Contents

Figures

1   Introduction

The inability of the stress intensity factor to account for some crack growth behaviours [1,2,3] is often attributed to its failure to acommodate plastic behaviour at the crack tip. This shortfall has driven the development of alternative crack characterisation parameters based on a more explicit consideration of crack tip plasticity ([4][5]). Importantly, it has also served to underscore the key role that plastic flow plays as a precursor to both the initiation and growth of fatigue cracks in ductile materials.

It is now well understood that the energy expended in deforming a ductile material is consumed in the production of heat and/or stored in processes of crystalline re-arrangement involving the formation and motion of dislocations and vacancies, and if crack growth occurs, an increase in surface energy. Energy storage is thought to be strongly related to fatigue damage; the most intuitive connection being that between crack growth and an increase in surface energy. Experimental studies over the past few decades have gone to some length in supporting this notion (see [6,7,8]), but the task of experimental verification has been fraught by the difficulty in measuring the relevant energy in a non-intrusive manner. Two techniques have traditionally been applied to energy measurement: annealing calorimetry and the single-step method [9]. The former entails the use of a calorimeter to measure the energy liberated by recrystallisation, where the stage in the annealing process at which the release occurs can assist in identifying the energy-release mechanism. However, in imposing a microstructural change, the method is not suited to applications where the aim is to track the evolution of stored energy as a function of exposure to cyclic loading. Better adapted to this task is the single-step method, where, based on energy conservation principles, the stored energy is inferred from measurement of the applied work and dissipated heat, viz.,

$$\Delta \dot{U} = \Delta \dot{W} - \Delta \dot{Q} \qquad (1)$$

where $\Delta \dot{U}$ is the rate of change of stored energy, $\Delta \dot{W}$ is the rate of change of supplied work, and $\Delta \dot{Q}$ is the rate of change of dissipated heat. The applied work is easily deduced from an appropriately measured force-strain curve. Evaluation of dissipated energy is an inherently more difficult exercise as it relies on the precise measurement of temperature at carefully chosen locations on the structure. Traditionally, the use of miniature thermistors or thermocouples for this task has necessitated the adoption of tenuous assumptions in the energy calculations, usually comprising the over-simplification of thermal boundary conditions and, in extreme cases, can limit investigations to circumstances where thermal equilibrium is established (see [10]).

Recent advances in infrared detection technology have greatly eased the burden of acquiring temperature measurements at the requisite precision for useful insitu assessments of dissipated energy. This report outlines an appropriate methodology that exploits the relatively recent innovation of focal-plane array infrared-detection technology. A numerical scheme is developed which facilitates the prediction of energy dissipation rates under transient conditions based on radiometric measurement of the surface temperature distribution. Although the scheme provides a framework for advancing research into the links between stored energy and fatigue damage, the experimental work described in this

report will focus only on the measurement of dissipated energy, with the aim of exploring the prospect of predicting crack-growth rates based solely on remote thermographic assessment of energy dissipation.

2 A Computational Scheme for Estimating Energy Dissipation from Temperature Measurements

The formulation given is an expansion to two-dimensions of the one-dimensional approach previously used [9] in a thermographic investigation of energy storage in a cylindrical specimen exposed to sustained cyclic loading. The starting point here is the heat-diffusion equation in two-dimensional rectangular coordinates,

$$\frac{\partial \theta}{\partial t} - \alpha\left(\frac{\partial^2 \theta}{\partial x^2} + \frac{\partial^2 \theta}{\partial y^2}\right) = \frac{\dot{q}}{\rho C}, \tag{2}$$

where θ is the temperature change, $\dot{q}$ is the power density, α is the thermal diffusivity, ρ is the density and C is the specific heat. The objective is to find an estimate for the power, $\dot{q}$, corresponding to some measured temperature response, a problem conveniently expressed in terms of the minimisation of an objective function $\mathcal{X}$,

$$\mathcal{X} = \iint_A (T - \theta)^2 \, dx \, dy, \tag{3}$$

where T is the measured temperature, θ is the temperature response associated with the unknown heat source, and A is the domain over which the solution is sought. Rewriting the objective function, (Eqn 3), to include the constraint that the undetermined temperature response, θ, satisfies the heat diffusion equation (Eqn 2), yields

$$\mathcal{X} = \iint_A (T - \theta)^2 \, dx \, dy - \lambda F, \tag{4}$$

$$F = \frac{\partial \theta}{\partial t} - \alpha\left(\frac{\partial^2 \theta}{\partial x^2} + \frac{\partial^2 \theta}{\partial y^2}\right) - \frac{\dot{q}}{\rho C}, \tag{5}$$

where λ is the Lagrange Multiplier and F is the constraint equation. In approaching the optimisation problem numerically, the objective function, Eqn 4, is more appropriately expressed in a discretised form, i.e.,

$$\mathcal{X} = \sum_{i,j}(T_{i,j} - \theta_{i,j})^2 - \lambda_{i,j}F_{i,j}, \tag{6}$$

where the subscripts i and j refer to nodal positions in the rectangular coordinates x and y respectively. The contraint, F, is discretised using a Crank-Nicolson scheme.

For the sake of simplicity and clarity in the following derivation, mesh spacings in the x and y directions are assumed equivalent ($\Delta y = \Delta x$). Accordingly, $F_{i,j}$ is written as,

$$F_{i,j} = (\frac{2\Delta x^2}{\alpha\Delta t} + 4)\theta_{i,j}^n - (\theta_{i+1,j}^n + \theta_{i-1,j}^n + \theta_{i,j+1}^n + \theta_{i,j-1}^n) - \frac{2\bar{q}_{i,j}}{K}\Delta x^2 -$$
$$(\theta_{i+1,j}^{n-1} + \theta_{i-1,j}^{n-1} + \theta_{i,j+1}^{n-1} + \theta_{i,j-1}^{n-1}) + (\frac{2\Delta x^2}{\alpha\Delta t} + 4)\theta_{i,j}^{n-1}, \tag{7}$$

Here, $n\Delta t$ is the time, K is the thermal conductivity, and $\bar{q}$ is the averaged power density over the time increment Δt, viz.,

$$\bar{q}_{i,j} = \frac{1}{\Delta t}\int_t^{t+\Delta t} \dot{q}_{i,j} \, \partial t. \tag{8}$$

For convenience, Eqn 2 is expressed in the following abbreviated form,

$$F_{i,j} = A\theta_{i,j}^n - (\theta_{i+1,j}^n + \theta_{i-1,j}^n + \theta_{i,j+1}^n + \theta_{i,j-1}^n) - B\bar{q}_{i,j} - C_{i,j}, \tag{9}$$

where,

$$A = (\frac{2\Delta x^2}{\alpha\Delta t} + 4), \tag{10}$$
$$B = \frac{2\Delta x^2}{K}, \tag{11}$$
$$C_{i,j} = (\theta_{i+1,j}^{n-1} + \theta_{i-1,j}^{n-1} + \theta_{i,j+1}^{n-1} + \theta_{i,j-1}^{n-1}) - (\frac{2\Delta x^2}{\alpha\Delta t} + 4)\theta_{i,j}^{n-1}. \tag{12}$$

Substituting Eqn 9 into Eqn 6 then yields,

$$\mathcal{X} = \sum_{i=2}^{N-1}\sum_{j=2}^{M-1}[(T_{i,j}-\theta_{i,j})^2 + \lambda_{i,j}(A\theta_{i,j} - (\theta_{i+1,j}+\theta_{i-1,j}+\theta_{i,j+1}+\theta_{i,j-1}) - B\bar{q}_{i,j} - C_{i,j})], \tag{13}$$

Differentiating $\mathcal{X}$ with respect to the unknowns θ, λ and $\bar{q}$, results in the following set of normal equations,

$$\frac{\partial\mathcal{X}}{\partial\lambda_{i,j}} = \sum_{i=2}^{N-1}\sum_{j=2}^{M-1} -A\theta_{i,j} + (\theta_{i+1,j} + \theta_{i-1,j} + \theta_{i,j+1} + \theta_{i,j-1}) + B\bar{q}_{i,j} + C_{i,j} = 0, \tag{14}$$

$$\frac{\partial\mathcal{X}}{\partial\theta_{i,j}} = \sum_{i=2}^{N-1}\sum_{j=2}^{M-1} -2(T_{i,j} - \theta_{i,j})\delta_{i,j} - A\lambda_{i,j} + \lambda_{i+1,j} + \lambda_{i-1,j} + \lambda_{i,j+1} + \lambda_{i,j-1} = 0, \tag{15}$$

$$\frac{\partial \mathcal{X}}{\partial \overline{q}_{i,j}} = \sum_{i=2}^{N-1} \sum_{j=2}^{M-1} -B\lambda_{i,j} = 0. \tag{16}$$

It is possible to show that the relevant stationary value is, as required, a minimum. Additionally, the linearity of the objective function ensures uniqueness of the solution. Consider now the solution of the normal equations (*Eqns 14-16*), which are expressed in the matrix form,

$$\mathbf{A}\overline{X} = \overline{Y}, \tag{17}$$

where $\mathbf{A}$ is a matrix of coefficients, and $\overline{X}$ and $\overline{Y}$ are vectors of the unknowns and forcing functions respectively. The heat source is expressed as a function of x and y with K terms, namely,

$$\overline{q}_{i,j} = (D_1, D_2, D_3, \ldots, D_K) \begin{pmatrix} P_{i,j,1} \\ P_{i,j,2} \\ P_{i,j,3} \\ \vdots \\ P_{i,j,K} \end{pmatrix}, \tag{18}$$

Here, D_i are the unknown regressor parameters and P_i are the regressor terms, which are described later. The vectors $\overline{X}$ and $\overline{Y}$ may then be written as,

$$\overline{X} = \left\{ \begin{array}{c} \theta_{2,2} \\ \theta_{2,3} \\ \cdot \\ \cdot \\ \cdot \\ \theta_{N-1,M-1} \\ \lambda_{2,2} \\ \lambda_{2,3} \\ \cdot \\ \cdot \\ \cdot \\ \lambda_{N-1,M-1} \\ D_1 \\ D_2 \\ \cdot \\ \cdot \\ \cdot \\ D_K \end{array} \right\}, \quad \overline{Y} = \left\{ \begin{array}{c} C_{2,2} - T_{2,1} - T_{1,2} \\ C_{2,3} - T_{1,3} \\ \cdot \\ \cdot \\ \cdot \\ C_{N-1,M-1} - T_{N,M-1} - T_{N-1,M} \\ 2\delta_{2,2}T_{2,2} \\ 2\delta_{2,3}T_{2,3} \\ \cdot \\ \cdot \\ \cdot \\ 2\delta_{N-1,M-1}T_{N-1,M-1} \\ 0 \\ \cdot \\ \cdot \\ \cdot \\ \cdot \\ 0 \end{array} \right\}. \tag{19}$$

The matrix $\mathbf{A}$ is written in the following compound form,

$$A = \begin{bmatrix} \mathbf{M_1} & \mathbf{M_2} & \overline{V}_1 \ldots \overline{V}_K \\ \mathbf{M_3} & \mathbf{M_1} & \mathbf{0} \\ \mathbf{0} & \begin{matrix} \overline{H}_1 \\ \vdots \\ \overline{H}_K \end{matrix} & \mathbf{0} \end{bmatrix}, \tag{20}$$

where $\mathbf{M_1}$, $\mathbf{M_2}$ and $\mathbf{M_3}$ are matrices and $\overline{H}_K$ and $\overline{V}_K$ are vectors comprising the regressor functional terms defined in *Eqn 18*.

It is worthwhile remarking on the structure of the component matrices. $\mathbf{M_1}$ simply comprises coefficients of the Crank-Nicolson problem defined earlier and requires no further comment. $\mathbf{M_2}$ includes conditions imposed to reconcile *Eqn 15* with the absence of θ on the boundaries, $i = 1, N$ and $j = 1, M$. This problem is resolved by expressing θ in terms of known values of T and defined values of λ. As an example, consider the boundary at $i = 1$. Noting that, like θ, λ is defined within the interior domain $i = 2, 3, \ldots, N - 1$, $j = 2, 3, \ldots, M - 1$, manipulation of *Eqn 17* yields the expression,

$$-2(T_{1,j} - \theta_{1,j}) + \lambda_{2,j} = 0, \tag{21}$$

from which,

$$\theta_{1,j} = T_{1,j} - \frac{1}{2}\lambda_{2,j}. \tag{22}$$

Repeating this for the other boundaries gives,

$$\begin{aligned} \theta_{N,j} &= T_{N,j} - \frac{1}{2}\lambda_{N-1,j}, \\ \theta_{i,1} &= T_{i,1} - \frac{1}{2}\lambda_{i,2}, \\ \theta_{i,M} &= T_{i,M} - \frac{1}{2}\lambda_{i,M-1}, \end{aligned} \tag{23}$$

and similarly for the corner points,

$$\begin{aligned} \theta_{1,1} &= T_{1,1} - \lambda_{2,2}, \\ \theta_{1,M} &= T_{1,M} - \lambda_{2,M-1}, \\ \theta_{N,1} &= T_{N,1} - \lambda_{N-1,2}, \\ \theta_{N,M} &= T_{N,M} - \lambda_{N-1,M-1}. \end{aligned} \tag{24}$$

M_3 is a modified identity matrix, where the diagonal values represent the weightings applied to the experimental data points. Should the need arise to exclude certain points from the analysis, this can be achieved by simply assigning a value of 0 to the appropriate diagonal element.

As stated earlier, the heat source functional terms appear in the vectors V and H, which for the kth term $^kP_{i,j}$, may be written as,

$$\overline{V}_k = -B^k\overline{P}_k = -B \begin{pmatrix} ^kP_{2,2} \\ ^kP_{2,3} \\ \vdots \\ ^kP_{N-1,M-1} \end{pmatrix}, \tag{25}$$

and,

$$\overline{H}_k = {}^k\overline{P}^T = \left({}^kP_{2,2}, {}^kP_{2,3}, \ldots, {}^kP_{N-1,M-1} \right). \tag{26}$$

Selection of an appropriate functional form for the terms ^kP should reflect the aims of the planned experimental work. It is important to emphasise that the objective in this study is not to recover the precise spatial distribution of the energy dissipation, but merely to measure the total crack-tip energy dissipation. In this limited context, a simple low-order form should suffice. A biquadratic expression was chosen, viz.,

$$\bar{q}(x,y) = D_1 x^2 + D_2 y^2 + D_3 xy + D_4 x + D_5 y + D_6, \tag{27}$$

which, in the form of *Eqn 18*, is written as,

$$\bar{q}_{i,j} = (D_1, D_2, D_3, D_4, D_5, D_6) \begin{pmatrix} x^2 \\ y^2 \\ xy \\ x \\ y \\ 1 \end{pmatrix}_{i,j}. \tag{28}$$

Testing of the scheme initially involved synthetic data produced from finite-difference modeling of an appropriate two-dimensional heat-dissipation problem. Estimates of the total power were obtained from several sets of synthetic data each augmented with a different amount of Gaussian noise. It was found that good estimates were produced even in the presence of unrealistically high levels of random noise, providing verification of the precision and robustness of the proposed scheme. As expected, the scheme was far more sensitive to systematic errors in the data. These tests also revealed that computations quickly become laborious with increased mesh size, due to the N^4 growth of the coefficient matrix. Fortunately, robustness was found to be excellent even with moderately sized meshes. Accordingly, a mesh of 10×10 was chosen for all subsequent experimental work.

2.1 Experimental Validation

An experimental test case was devised to facilitate the practical verification of the outlined scheme. *Figure 1* shows the experimental set-up, the salient aspect of which is the use of a Peltier cell applied to the back face of an aluminium sample to simulate the effect of an internal heat source. Temperature response data were acquired through inspection of the front-face with a focal-plane array infrared imager (described in more detail shortly). Several different Peltier-cell power settings were considered. In each case, before acquiring data, a resting period of 5 minutes was allowed to accommodate the re-establishment of thermal equilibrium. This was necessary to facilitate the independent computation of the effective power dissipation, achieved by integration of the normal temperature gradient along a closed contour surrounding the zone of heat production (see *Figure 2*). At steady state, it can be shown that,

$$\iint_{\mathbf{A}} \dot{q}(x, y) \, dA = \oint_{\mathbf{C}} -K \frac{\partial T}{\partial n} ds, \tag{29}$$

where $\partial/\partial n$ denotes differentiation in the direction of the outward normal to the circuit path and ds is an infinitesimal segment along the contour $\mathbf{C}$. Estimates derived from the optimisation scheme were found to agree well with those derived through contour integration. The comparison in *Figure 3* for 7 different nominal power settings shows a discrepancy that, in the worst case, amounts to less than two standard-deviations of the respective optimisation result.

3   Experimental Procedure

Single-edge notched specimens were manufactured from a low-carbon steel, and used in the as-recieved condition. Two configurations were considered, shown in *Figure 4* as type-A and type-B. The fatigue testing involved sinuisoidal loading at a fixed frequency of 12.5 Hz, an R-ratio of 0.1 and a mid-section stress amplitude of 122 MPa. As already stated, temperature measurements were acquired with an infrared imager. Its salient feature is a mechanically cooled 512×512 Platinum Silicide photonic detector with a rated noise equivalent temperature detectivity of 150 mK and a fixed frame rate of 25 Hz.

3.1 Analysis of the Cyclic Plastic Zone Size

Initial experimental work focused on mapping the cyclic plastic zone produced during crack growth at the stipulated loading levels. This was done to facilitate selection of a suitable mesh spacing for the optimisation algorithm so that the entire crack-related heat-production zone could be encompassed within the 10×10 computational grid used in the analysis.

Fortunately, thermography affords a number of means by which to map the extent of cyclic plastic deformation in a material. An obvious approach is to apply the optimisation scheme to a growing region of data centred on the crack tip with the expectation that an
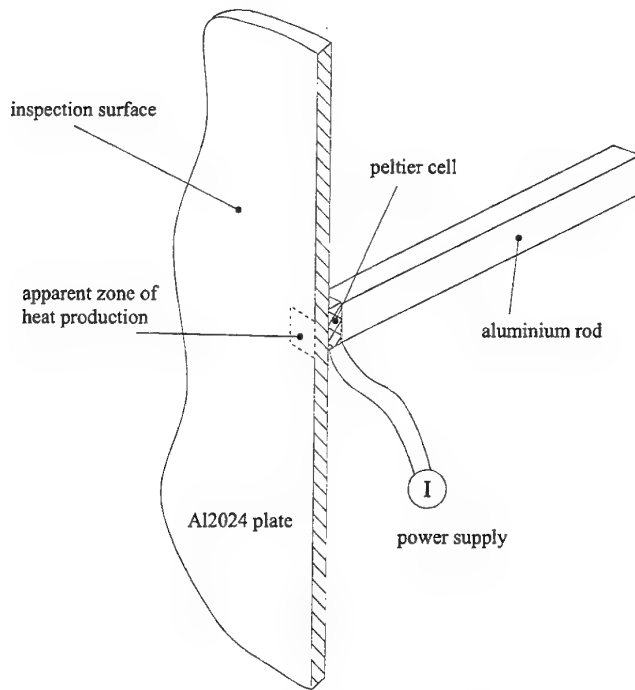
Figure 1: *Schematic of experimental set-up used for validation of the energy computation scheme. Note that the Aluminium rod serves as a conduit for the flow of heat from a large thermal mass (not shown) to the Aluminium plate.*
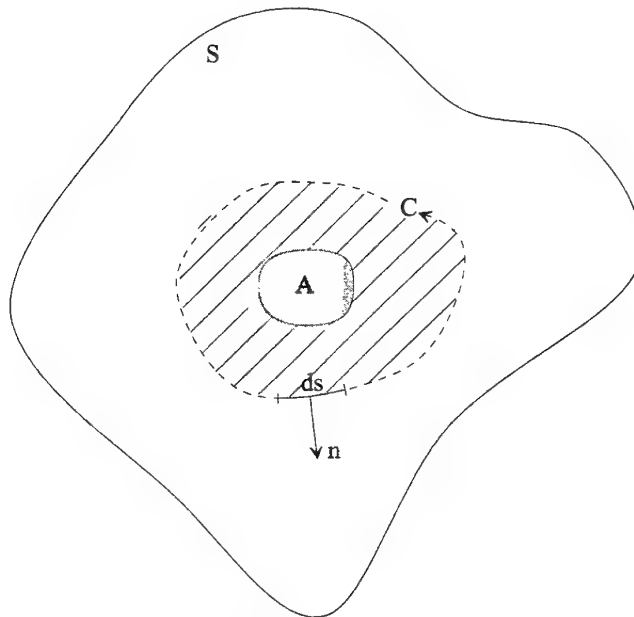

Figure 2: *Contour of integration for the evaluation of the power density within region* **A**
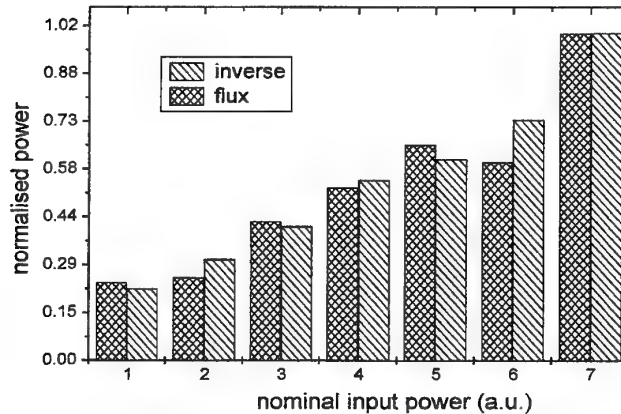
Figure 3: Comparison between the flux-based and inverse estimates for the heat source
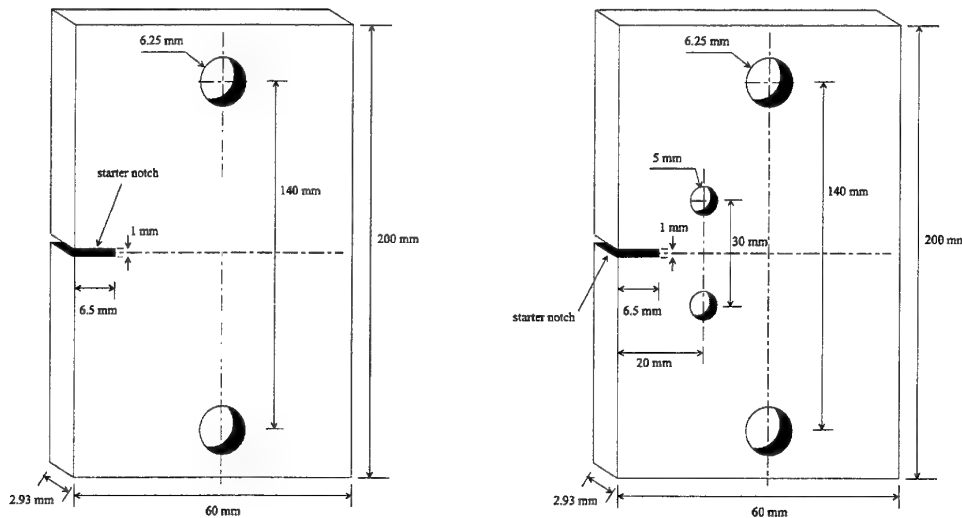

Figure 4: Schematic showing type-A (left) and type-B specimen geometries.

expansion of this region beyond that which fully contains the heat-production zone would produce no further increase in estimated total power. Although likely to be successful, the approach is time consuming. A more expedient alternative is to presume that heat production occurs wherever a significant temperature increase is recorded. This of course ignores the effect of heat conduction, which will tend to overstate the actual zone-size.

The method adopted here was to use the second harmonic thermal response, which is that component of the measured thermal response that occurs at twice the loading frequency. The reason for its use is two-fold. The process of mapping the second harmonic response is simple and relatively fast, usually achieved in under a minute. And secondly, the technique is likely to be effective since, due to its inherent non-linearity, cyclic plastic deformation should manifest a much higher second harmonic response (as well as higher harmonics) than regions undergoing purely elastic loading.

Measurement of the second harmonic component was achieved by performing at each
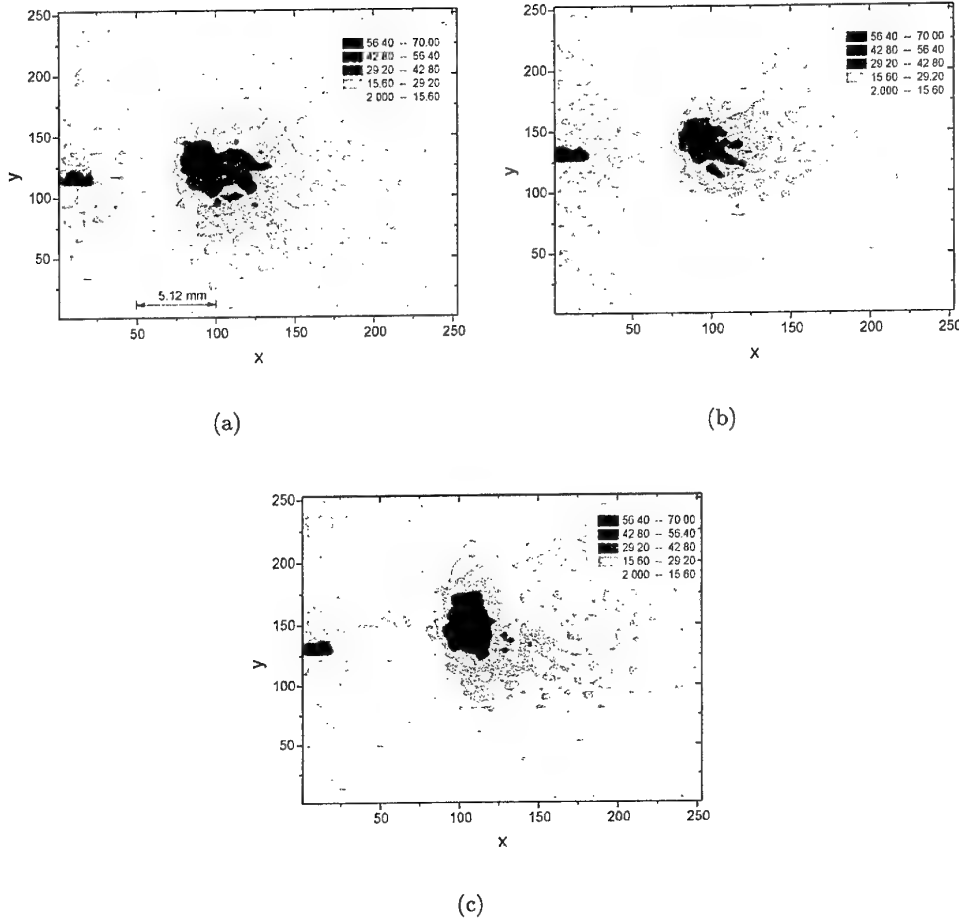
(a)

(b)

(c)

Figure 5: Variation in measured second harmonic response due to the application of an overload. Crack propagation direction is from left to right.

pixel location a real-time cross-correlation between the measured infrared response and the square of the load signal. At a 12.5 Hz loading frequency, the second harmonic response occurs at 25 Hz which coincides with the camera sampling frequency and would result in severe aliasing. To avoid this, loading was applied at a lower frequency of 10 Hz. Since the phase difference between the temperature and strain evolutions is a *priori* unknown, both in-phase and quadrature components of the correlation were obtained, yielding a resultant,

$$R_{i,j} = \sqrt{(I_{i,j}^2 + O_{i,j}^2)} \qquad (30)$$

where I and O are respectively the in-phase and quadrature components of the cross-correlation. *Figure 5* shows a sequence of maps of the resultant acquired in relation to an experiment where a sample exposed to persistent cyclic loading was suddenly subjected to an overload.

10

The three images (*Figure 5*) relate, respectively, to a time (a) prior to application of the overload, (b) immediately following the overload, and (c) at a stage where the crack had grown a further 2 mm in length. Variations in the size of the cyclic plastic zone, as inferred from the second harmonic response measurements, are broadly consistent with the effects understood to follow the application of overload. The reduction recorded from images (a) to (b) for example are consistent with one or a combination of the following overload induced mechanisms (see [11]): compressive residual stress, crack tip blunting and crack closure. The subsequent expansion in zone size from (b) to (c) is consistent with the crack having grown through the overload affected zone.

Based on these second harmonic response measurements, an analysis window of 11 mm × 11 mm was deemed sufficiently large to encompass the anticipated cyclic plastic zone size, and accordingly was used for all subsequent experimental work.

4 RESULTS

4.1 Specimen type-A

Seven single-edge notched specimens were fatigue-tested under the loading regime described earlier. Temperature response data were acquired at irregular but frequent intervals during the fatigue test and the energy dissipation calculations performed off-line at the completion of the testing program. *Figure 6* shows the evolution in computed power as a function of crack length for all of the tested samples. The upward monotonic trend evident here is intuitive and consistent with the intensification and enlargement of the region of cyclic plastic deformation which is expected as the stress amplitude increases with crack growth under constant amplitude loading.
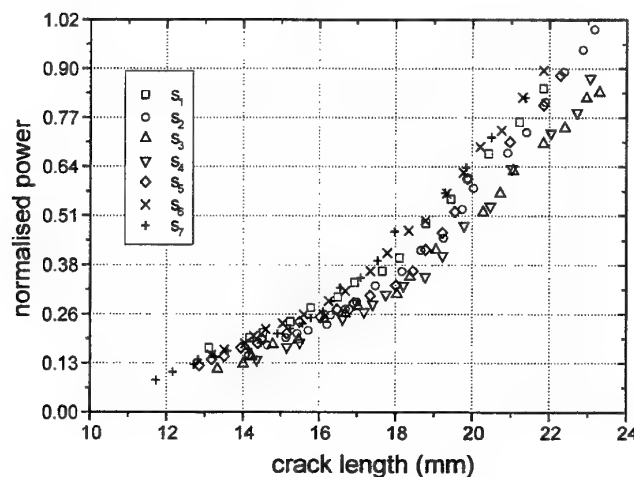

Figure 6: Dissipated power as a function of crack length for type-A geometry

More noteworthy is the apparent linear relationship between the power and crack growth rate (*Figure 7*). Several earlier studies that have explored the relationship between energy and fatigue in metals (see for example [9]) have raised the possibility that

structural failure of an element of material may occur when the stored energy reaches a certain 'critical' level characteristic of the material. If, in the present study, cyclic plastic deformation occurred with a constant dissipation function, then the observed linear trend would support this assertion. Since there was no measure of the applied mechanical work here, no assessment of the dissipation function could be made, and so the link is largely speculative. It does however encourage further investigation.

Considering once again the result shown in *Figure 7* it is notable that an extrapolation of the best-fit trend passes almost precisely through the origin. From an intuitive standpoint this seems reasonable in suggesting that crack growth cannot occur without energy dissipation. Again, it has not been possible to experimentally verify whether the relationship does indeed hold as the crack growth rate approaches zero. Attempts were made to do this, however it became apparent that a much improved detector sensitivity would be required for success in testing under these conditions.
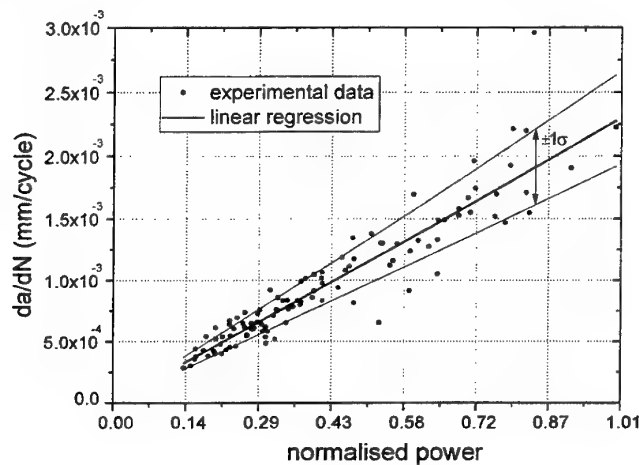

Figure 7: Dissipated power as a function of crack growth rate for the type-A specimen. Error band corresponds to one standard deviation of the data.

It is worthwhile commenting on the increasing scatter as a function of crack growth rate. This is presumed to arise in part as a result of the increased uncertainty in the measurement of crack length with increased rate of crack growth.

4.2 Specimen type-B

The type-B specimen design was conceived to provide a simple means to test for the effect of specimen geometry on the previously established linear relationship. The results (*Figure 8*) indicate a marked deviation in the evolution of the energy dissipation rate as a function of crack length over that recorded for the type-A configuration. A reduction in the net cross-sectional area is expected to lead to higher crack-tip stresses, and consequently to greater crack-tip plasticity at most crack lengths, which is supported by the data. Despite the clear distinction here between the two sets of results, the variation in the rate of heat-dissipation with crack growth rate (*Figure 9*) appears largely unchanged.
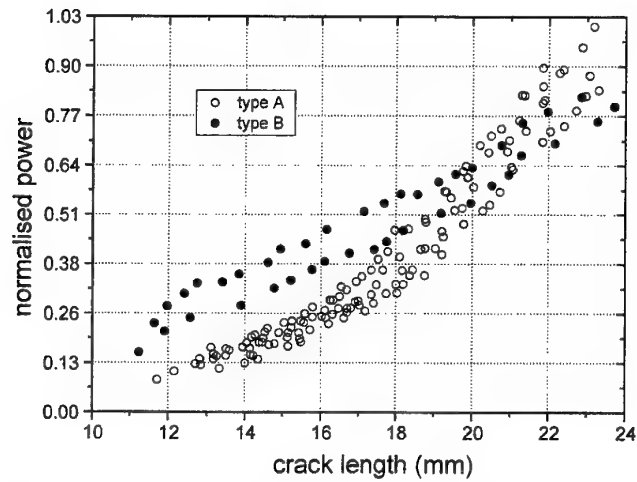
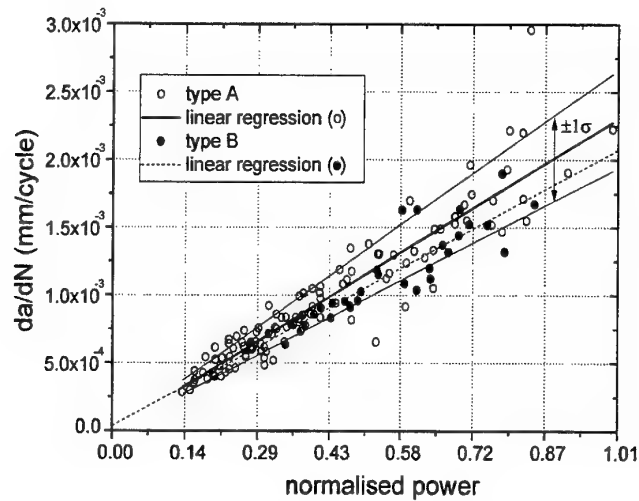*Figure 8: Dissipated power as a function of crack length for type-A and type-B specimens.*

Figure 9: Dissipated power as a function of crack growth rate for type-A and type-B specimens.

4.3 Specimen type-A with Overload

Load interaction effects caused by complex loading are known to play an important role in dictating crack growth behaviour. In a preliminary attempt to assess the impact of such events on the relationship between heat dissipation and crack growth rate, tests were conducted on the type-A geometry where a constant amplitude loading sequence (described earlier) was augmented with a single overload event applied at a nominal crack length of 15 mm. Prior experimentation had revealed that a static load 30% higher than the peak cyclic load would lead to the formation of a substantial monotonic plastic zone surrounding the crack tip (see *Figure 10*), and consequently facilitate crack closure and the formation of a zone of compressive residual stress.

Figure 10: Monotonic plastic zone size produced by a 30% overload event.

Figure 11 demonstrates an immediate and significant impact relating to the overload event. Initially, the energy dissipation rate is suppressed relative to that recorded under benchmark conditions, maintaining a steady value as a function of crack length for approximately 3 mm of crack growth. This is followed by a period of rapid ascent in dissipation rate, which, by the end of testing, slightly exceeds that recorded in the absence of overload. *Figure 12* compares the dissipation rate to the rate of crack growth. The increase in scatter associated with the computation of crack growth rate, combined with the relatively small data set limits the scope of comment possible here. Although the data does suggest that load interaction effects are likely to play an important role in this relationship, it is difficult to speculate on the physical mechanisms at work. For instance, the presence of compressive residual stress is known to supress the rate of crack growth to levels below that predicted by a stress-intensity factor calculation, leading to so-called anomolous behaviour. Measurements of energy dissipation however should, unlike the stress intensity factor, reflect the presence of a compressive residual stress since the level of cyclic plastic deformation is also suppressed, in essence leading to some level of cancellation. Clearly, this is mere speculation and cannot be tested with the available data, but is nevertheless an interesting possibility worth further investigation.
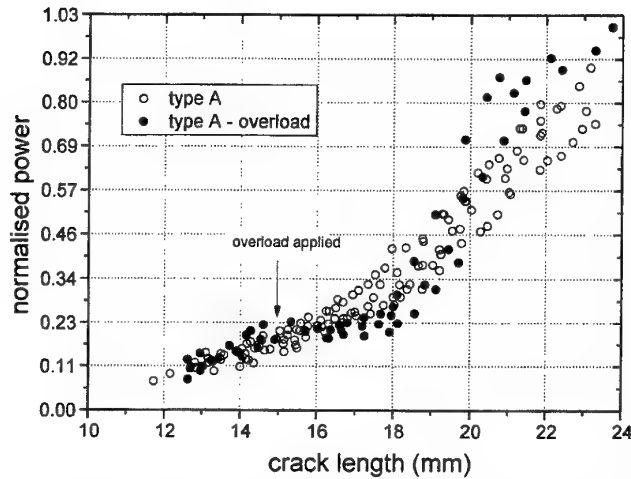
Figure 11: Dissipated power as a function of crack length for the type-A configuration with and without overload.
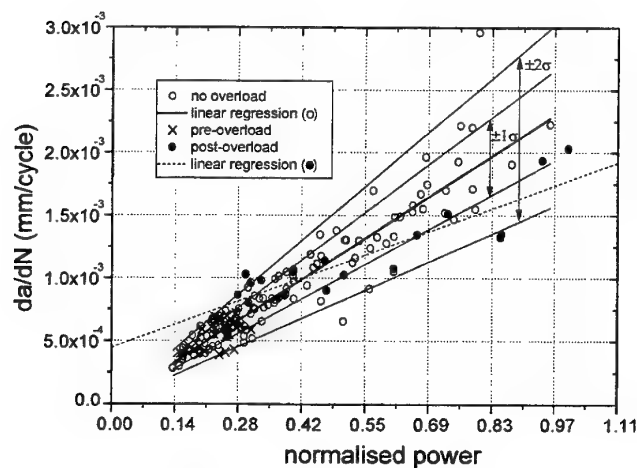
Figure 12: Dissipated power as a function of crack growth rate for the type-A configuration with and without overload.

5   CONCLUSION

A numerical scheme has been presented to allow for the remote assessment of the energy dissipation associated with crack-growth in metals on the basis of remote radiometric temperature measurement. After providing experimental verification of the scheme, it was applied in an investigation of the relationship between energy dissipation and the rate of crack growth in mild steel exposed initially to constant amplitude cyclic loading. A linear relationship was found and then reaffirmed in tests on a more complex geometry, indicating some level of geometry independence, an encouraging result from the standpoint of developing a useful crack characterisation parameter. The relationship did not appear to be maintained when load interaction effects were included by means of a static overload, suggesting that other factors not considered in the present study are involved.

Acknowledgements

References

1. J. Schijve, J. Backland, A. Blom, and C. J. Beevers (1982). *Fatigue Thresholds*, **2**, EMAS, Warley, 881.

2. B. N. Leis and T. P. Forte (1981). Fatigue Growth of Initially Physically Small Cracks in Notched Aluminum and Steel Plates, *Fracture Mechanics, ASTM STP 743, Philadelphia*, 100–124.

3. S. Suresh (1983). Micromechanisms of Fatigue Crack Growth Retardation Following Overloads, *Engineering Fracture Mechanics*, **18**, 577–593.

4. D. Broek (1985). A similitude Criterion for Fatigue Crack Growth Modelling, *Fracture Mechanics: Sixteenth Symposium, ASTM STP* 868, 347–360.

5. G. C. Sih (1980). Prediction of Crack Growth Characteristics, *Proc. Int. Symp. Strain Energy Density Criterion, Hungary*, 3–16.

6. M. B. Bever, D. L. Holt and A. L. Titchener (1973). The Stored Energy of Cold Work, *Prog. Mater. Sci.*, **17**.

7. S. E. Gurevich and A. P. Gaevoi (1973). Method of Experimentally Determining Rupture Energy in Cyclical (Fatigue) Loading, *Zavodskaya Laboratoriya*, **39**, 1110–1114.

8. R. V. Romashov and V. V. Fedorov (1975). Method of Experimentally Checking Thermodynamic Ideas on the Failure of a Solid Body During Fatigue Tests, *Zavodskaya Laboratoriya*, **41**, 229–232.

9. A. K. Wong and G. C. Kirby (1990). A Hybrid Numerical/Experimental Technique for Determining the Heat Dissipated During Low Cycle Fatigue, *Engineering Fracture Mechanics*, **37**, pp. 493–504.

10. T. S. Gross and J. Weertman (1982). Calorimetric Measurement of the Plastic Work of Fatigue Crack Propagation in 4140 Steel, *Metallurgical Transactions A*, **13A**, pp. 2165–2172.

11. S. Suresh (1982). Crack Growth Retardation Due to Micro-Roughness: A Mechanism for Overload Effects in Fatigue, *Scripta Metallurgica*, **16**, pp. 995–999.

12. D. M. Corlby and P. F. Packman (1973). On the Influence of Single and Multiple Overloads on Fatigue Crack Propagation in 7075-T6511 Aluminium, *Engineering Fracture Mechanics*, **5**, pp. 479–497.

12. R. E. Jones (1973). Fatigue Crack Growth Retardation After Single Cycle Peak Overload in Ti-6Al-4V Titanium Alloy, *Engineering Fracture Mechanics*, **5**, pp. 585–604.

DISTRIBUTION LIST

Thermographic Assessment of the Heat Dissipation Associated with Fatigue Crack
Growth in Mild Steel

N. Rajic

Number of Copies

DEFENCE ORGANISATION

S&T Program

Chief Defence Scientist	
FAS Science Policy	
AS Science Corporate Management	1
Director General Science Policy Development	
Counsellor, Defence Science, London	Doc Data Sht
Counsellor, Defence Science, Washington	Doc Data Sht
Scientific Adviser to MRDC, Thailand	Doc Data Sht
Director General Scientific Advisers and Trials	
Scientific Adviser Policy and Command	1
Navy Scientific Adviser	Doc Data Sht
Scientific Adviser, Army	Doc Data Sht
Air Force Scientific Adviser	1
Director Trials	1

Aeronautical and Maritime Research Laboratory

Director, Aeronautical and Maritime Research Laboratory	1
Chief, AED	1
RLACS	1
N. Rajic	5
S. Lamb	1

DSTO Libraries

Library Fishermens Bend	2
Library Salisbury	1
Australian Archives	1
Library, MOD, Pyrmont	Doc Data Sht

Capability Development Division

Director General Maritime Development	Doc Data Sht
Director General Land Development	Doc Data Sht
Director General C3I Development	Doc Data Sht

Intelligence Program

Defence Intelligence Organisation	1

Library, Defence Signals Directorate	Doc Data Sht

Acquisition Program

Corporate Support Program (libraries)

Officer in Charge, TRS, Defence Regional Library, Canberra	1
Officer in Charge, Document Exchange Centre	1
Additional copies for DEC for exchange agreements	
US Defense Technical Information Center	2
UK Defence Research Information Centre	2
Canada Defence Scientific Information Service	1
NZ Defence Information Centre	1
National Library of Australia	1

UNIVERSITIES AND COLLEGES

Australian Defence Force Academy Library	1
Head of Aerospace and Mechanical Engineering, ADFA	1
Deakin University Library, Serials Section (M List)	1
Senior Librarian, Hargrave Library, Monash University	1
Librarian, Flinders University	1

OTHER ORGANISATIONS

NASA (Canberra)	1
Australian Government Publishing Service	1

ABSTRACTING AND INFORMATION ORGANISATIONS

INSPEC: Acquisitions Section Institution of Electrical Engineers	1
Library, Chemical Abstracts Reference Service	1
Engineering Societies Library, US	1
Materials Information, Cambridge Science Abstracts, US	1
Documents Librarian, The Center for Research Libraries, US	1

INFORMATION EXCHANGE AGREEMENT PARTNERS

Acquisitions Unit, Science Reference and Information Service, UK	1
Library – Exchange Desk, National Institute of Standards and Technology, US	1

SPARES

DSTO Salisbury Research Library	5

Total number of copies:	46

DEFENCE SCIENCE AND TECHNOLOGY ORGANISATION DOCUMENT CONTROL DATA	1. CAVEAT/PRIVACY MARKING

2. TITLE	3. SECURITY CLASSIFICATION
Thermographic Assessment of the Heat Dissipation Associated with Fatigue Crack Growth in Mild Steel	Document (U) Title (U) Abstract (U)

4. AUTHOR	5. CORPORATE AUTHOR
N. Rajic	Aeronautical and Maritime Research Laboratory 506 Lorimer St, Fishermans Bend, Victoria, Australia 3207

6a. DSTO NUMBER DSTO–TR–1190	6b. AR NUMBER 011-962	6c. TYPE OF REPORT Technical Report	7. DOCUMENT DATE August, 2001

8. FILE NUMBER M1/9/978	9. TASK NUMBER DST 01/122	10. SPONSOR CDS	11. No OF PAGES 17	12. No OF REFS 13

13. URL OF ELECTRONIC VERSION	14. RELEASE AUTHORITY
http://www.dsto.defence.gov.au/corporate/ reports/DSTO–TR–1190.pdf	Chief, Airframes And Engines Division

15. SECONDARY RELEASE STATEMENT OF THIS DOCUMENT

Approved For Public Release

OVERSEAS ENQUIRIES OUTSIDE STATED LIMITATIONS SHOULD BE REFERRED THROUGH DOCUMENT EXCHANGE, PO BOX 1500, SALISBURY, SOUTH AUSTRALIA 5108

16. DELIBERATE ANNOUNCEMENT

No Limitations

17. CITATION IN OTHER DOCUMENTS

No Limitations

18. DEFTEST DESCRIPTORS

Nondestructive tests	Thermography
Crack propagation	Fatigue (materials)
Cracking (Fracturing)	Cyclic loading
Remote detectors	Steels

19. ABSTRACT

This report examines the feasibility of predicting rates of crack growth in mild steel based on an evaluation of the crack tip dissipated energy. A numerical scheme is developed to provide a basis for the computation of dissipated power from measurements of temperature acquired using remote infrared detection. An experimental study is then described where measurements of crack-growth rate in mild-steel coupons exposed to constant amplitude cyclic loading are related to calculations of power dissipation. A simple linear relationship is indicated, with testing also providing some evidence of geometry independence, a key finding with regard to the possible use of dissipated energy as a fatigue characterisation parameter. However, further testing involving a more complex loading sequence led to a noticeable change in relationship indicating that the heat dissipation rate is unlikely to offer a simple basis for the prediction of crack growth rate under all loading conditions.